

# Auger-electron cascades in diamond and amorphous carbon

Beata Ziaja,<sup>1,2,3,\*</sup> David van der Spoel,<sup>1,†</sup> Abraham Szöke,<sup>1,4,‡</sup> and Janos Hajdu<sup>1,§</sup>

<sup>1</sup>*Department of Biochemistry, Biomedical Centre, Box 576, Uppsala University, S-75123 Uppsala, Sweden*

<sup>2</sup>*Department of Theoretical Physics, Institute of Nuclear Physics, Radzikowskiego 152, 31-342 Cracow, Poland*

<sup>3</sup>*High Energy Physics, Uppsala University, P.O. Box 535, S-75121 Uppsala, Sweden*

<sup>4</sup>*Lawrence Livermore National Laboratory, Livermore, California 94551*

(Received 6 June 2001; published 12 November 2001)

We have analyzed cascades of secondary electrons in diamond and amorphous carbon generated by the thermalization of a single Auger electron. The elastic electron mean free path was calculated as a function of impact energy in the muffin-tin potential approximation. The inelastic scattering cross section and the energy loss of electrons (expressed in terms of the differential inverse mean free path) were estimated from two “optical” models that utilize the measured dielectric constants of the materials. Using these data, a Monte Carlo model describing the time evolution of the cascade was constructed. The results show that at most around 20–40 secondary cascade electrons are released by a single Auger electron in a macroscopic sample of diamond or amorphous carbon. Consideration of the real band structure of diamond reduces this number further. The release of the cascade electrons happens within the first 100 fs after the emission of the primary Auger electron. The results have implications to planned experiments with femtosecond x-ray sources.

DOI: 10.1103/PhysRevB.64.214104

PACS number(s): 79.20.Hx, 82.53.Ps, 61.80.-x

## I. INTRODUCTION

Radiation damage prevents the structure determination of single biomolecules and other nonrepetitive structures at high resolutions in standard electron or x-ray scattering experiments.<sup>1</sup> Cooling can slow down sample deterioration, but it cannot eliminate damage-induced sample movement within the time needed to complete conventional measurements.<sup>1–3</sup> Emerging new x-ray sources, like free-electron lasers (FEL's),<sup>4,5</sup> will offer new possibilities in imaging. Analysis of the dynamics of damage formation on a sample in an x-ray FEL beam suggests that the conventional damage barrier (about 200 x-ray photons/Å<sup>2</sup> at 12 keV energy) (Ref. 2) may be extended substantially at very high dose rates and very short exposure times.<sup>6,7</sup> A new dynamic barrier of radiation tolerance has been identified at extreme dose rates and ultrashort exposure times.<sup>4–7</sup> This barrier is several orders of magnitude higher than previous theoretical limits in conventional experiments. The calculations show that at these extremes, sections of molecular transforms from single macromolecules may be recorded without the need to amplify scattered radiation through Bragg reflections.<sup>4,6</sup>

At 1 Å wavelength, about nine-tenths of the interacting photons will deposit energy into a biological sample, causing damage mainly through the photoelectric effect. The departing photoelectron leaves a hole in a low-lying orbital, and an upper-shell electron falls into it. This electron may either emit an x-ray photon to produce x-ray fluorescence or may give up its energy to another electron, which is then ejected from the ion as an Auger electron. The probability of fluorescence emission or Auger emission depends on the binding energy of the electron. In biologically relevant light elements, the predominant relaxation process (>99%) is through Auger emission, and most photoelectric events ultimately remove two electrons from these elements (C, N, O, S). The two electrons have different energies and leave the

atom at different times (for a more detailed description, see Refs. 6, 8 and 9).

In very small samples (like atoms and single molecules), the primary photoelectrons and the Auger electrons may escape from the sample without further interactions. However, in larger samples, these electrons will become trapped and thermalized. Thermalization involves inelastic electron-atom interactions, producing secondary cascade electrons. Here we analyze the specific contribution of Auger electrons to the ionization of a macroscopic sample through secondary cascade processes. We selected two different carbon compounds (diamond and amorphous carbon) as models for the calculations.

Auger electrons and photoelectrons propagate through the medium in a different manner. Their de Broglie wavelengths are  $\lambda_{\text{Auger}} \approx 0.8$  Å and  $\lambda_{\text{photoel}} \approx 0.1$  Å, respectively, and  $\lambda_{\text{Auger}}$  is comparable with atomic size. This implies that Auger electrons interact multiply with neighboring atoms, while moving through the system of atoms in the solid.<sup>10</sup> Moreover, since the energy of Auger electrons is low (around 0.25 keV), the interaction potential must include a nonlocal exchange term which makes an accurate description of the interaction complicated. In contrast, photoelectrons propagate almost freely through the medium, and their interaction with (single) atoms in the medium is well described by the Born approximation.<sup>11,12</sup> Therefore, in samples of intermediate size the low-energy Auger electrons are more likely to cause significant ionization than the higher-energy photoelectrons. The energy dependence of the mean free path (MFP) of electrons<sup>13,14</sup> in carbon implies that the MFP of a photoelectron is of the order of hundred angstroms whereas the MFP for the Auger electron is only a few angstroms ( $\geq 4$  Å). This implies that in samples of intermediate size a photoelectron scatters only a few times before leaving the interaction region, while the Auger electron will have multiple interactions.

In Sec. II we quantify the elastic and inelastic interactions

of Auger electrons with atoms within a solid. Using a Monte Carlo (MC) simulation we then model the secondary-electron cascade caused by inelastic interactions of the primary electron and subsequent secondary electrons with atoms. In Sec. III, the results of 500 computer simulations of different cascades are presented. These results give the estimated average ionization rate as a function of time. Finally, in Sec. IV we list our conclusions.

## II. SECONDARY ELECTRON CASCADE IN A SOLID

Our study of secondary-electron effects was performed for two forms of carbon: diamond ( $\rho = 3.51 \text{ g/cm}^3$ ) and graphite-like amorphous carbon ( $\rho = 2.21 \text{ g/cm}^3$ ).

Low-energy electrons ( $E \approx 250 \text{ eV}$ ) may undergo elastic and inelastic collisions with atoms (electrons and nuclei) in a solid. Since the corresponding electron wavelength is comparable with atomic dimensions, multiple scattering of electrons<sup>15</sup> on neighboring atoms have to be calculated quantum mechanically (QM). The QM exchange terms must then be incorporated into the interaction potential.

### A. Elastic scattering

Calculation of elastic scattering amplitudes and angular distributions can be done accurately by the partial-wave expansion technique.<sup>11,12</sup> In particular, the differential elastic cross-section ( $d\sigma_{el}/d\theta$ )( $E$ ) for the scattering of an electron on the atom is expressed, using the phase shift  $\delta_l$  of each partial wave, as follows<sup>11,12</sup>:

$$\frac{d\sigma_{el}}{d\theta}(E) = \frac{2\pi}{k^2} \left| \sum_{l=0}^{\infty} (2l+1) \sin(\delta_l) P_l(\cos(\theta)) \right|^2, \quad (1)$$

where  $k$  is the wave number, corresponding to the electron impact energy  $E$ ,  $P_l(\cos(\theta))$  denotes the Legendre polynomial of order  $l$ ,  $\theta$  is the scattering angle, and the sum goes over all partial-wave contributions  $l=0, \dots, \infty$ . The total elastic cross section  $\sigma_{el}(E)$  may be obtained from Eq. (1) by integration over  $\theta$ . The corresponding elastic mean free path (EMFP)  $\lambda_{el}$  (Refs. 13 and 16) can be calculated as

$$\lambda_{el}^{-1}(E) = N \sigma_{el}(E), \quad (2)$$

where  $N$  denotes the atomic density in the solid. In order to obtain the phase shifts  $\delta_l$  in Eq. (1), one should solve the respective radial wave equations for each partial wave with the approximate form of the exchange potential. To perform these calculations we used programs from the Barbieri/Van Hove Phase Shift package.<sup>17</sup> First we determined the radial charge density for a free atom, then calculated the radial muffin-tin potential<sup>10,15</sup> for atoms embedded in a solid (using various approximations to the exchange potential), and finally derived phase shifts from the muffin-tin potential. Multiple elastic scattering within a finite cluster, provided the resulting amplitude was large enough, was included in the calculations. Figure 1 shows the resulting EMFP for diamond and amorphous carbon. For large energies, the EMFP's for both diamond and amorphous carbon increase linearly with electron impact energy. They also scale properly with the

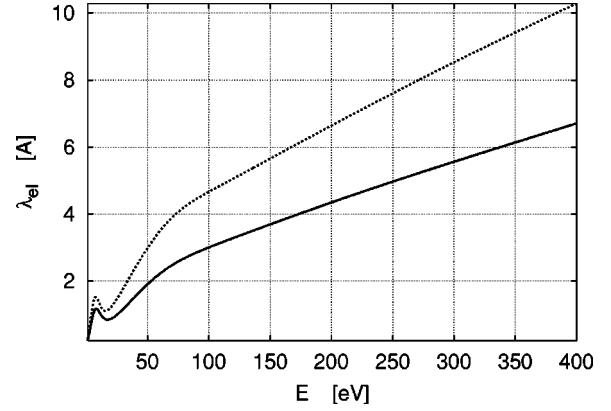


FIG. 1. Elastic mean free path ( $\lambda_{el}$  or EMFP) of electrons in diamond or amorphous carbon plotted as a function of electron energy  $E$ . Solid line corresponds to the EMFP of electron in diamond; dotted line shows the EMFP of electron in amorphous carbon.

medium density,  $\lambda_{el,diamond}(E)/\lambda_{el,carbon}(E) \approx \rho_{carbon}/\rho_{diamond}$  (cf. Refs. 14 and 18). With decreasing energy the EMFP's decrease monotonically until they show oscillatory features due to interference between low-order scattering waves.

### B. Inelastic scattering

An accurate treatment of inelastic atom-electron collisions in a solid is more difficult, especially in the case of low-energy Auger electrons when multiple scattering is important. In fact, a fully rigorous method for including inelastic scattering is not available so far. Following Fermi's work,<sup>19</sup> the passage of a fast charged particle was treated through the linear perturbation caused by its electric field in the solid. Subsequent developments<sup>20–25</sup> made it possible to extend the dielectric formulation in order to provide a more comprehensive description of quantum-mechanical effects in solids.

Generally speaking, the linear response of a solid is described by a generalized dielectric constant  $\epsilon(\mathbf{q}, \omega)$ , which depends on both momentum  $\hbar\mathbf{q}$  and frequency  $\omega$ . In quantum mechanics  $\hbar\omega$  corresponds to the energy transfer of the incident charged particle to the solid and  $\hbar\mathbf{q}$  to its momentum transfer.

It was shown<sup>23</sup> that the imaginary part of the dielectric constant,  $\text{Im}[-\epsilon(\mathbf{q}, \omega)^{-1}]$ , determines the energy loss of the test charge per unit time,  $dE/dt$ , by the formula  $dE/dt \sim \int d\mathbf{q} \int d\omega \text{Im}[-\epsilon(\mathbf{q}, \omega)^{-1}]$ . Therefore  $\text{Im}[-\epsilon(\mathbf{q}, \omega)^{-1}]$  is often called the energy loss function (ELF). It satisfies the oscillator-strength sum rule,<sup>18</sup> which relates the total energy loss to an effective number of free electrons per atom,  $Z_{eff}$ :

$$Z_{eff} = \frac{2}{\pi \hbar^2 \Omega_P^2} \int_0^\infty dE E \text{Im}[-\epsilon(\mathbf{q}, E/\hbar)^{-1}], \quad (3)$$

where  $\Omega_P = \sqrt{(4\pi n_a e^2)/m_e}$ ,  $n_a = N_A \rho/A$  is the density of atoms,  $N_A$  is Avogadro's number,  $\rho$  is the density of the solid,  $A$  is the atomic weight, and  $E$  is the energy loss of the incoming test particle.

The energy loss of Auger electrons in a solid is dominated by the excitation of plasmons. At first, we expect this behavior in metals, where conduction electrons form a jelliumlike plasma, but not in good insulators. Nevertheless, in all solids the energy loss is dominated by the excitation of valence electrons to the conduction band. The excited electron, in turn, interacts strongly with all other valence electrons. The resultant eigenstate is a plasma resonance. A more familiar result of similar interactions among atoms in a solid is the formation of optical phonons. As expected, the plasmon interacts strongly with the incident Auger electron. For a more quantitative explanation, let us examine the dielectric function  $\epsilon(\mathbf{q}, \omega)$ . It shows the importance of collective modes for the energy loss of charged particles. If one rewrites  $\epsilon = \epsilon_1 + i\epsilon_2$ , then  $\text{Im}[-\epsilon^{-1}] = \epsilon_2/(\epsilon_1^2 + \epsilon_2^2)$ . Since  $\epsilon_2$  is small, if  $\epsilon_1$  goes to 0 at a certain frequency  $\omega = \omega_p$ , the ELF  $\text{Im}[-\epsilon^{-1}]$  peaks sharply at this frequency. This corresponds to the excitation of plasma modes of frequency  $\omega_p$  by the incoming particle. Therefore, approximating the solid as a gas of free electrons models the electron energy loss well. As the width of the plasma resonance and its amplitude depend on the details of the plasmon coupling and its decay, accurate results can be expected only from detailed simulations.

In this paper we apply the Lindhard dielectric function approach together with optical-data models. The approximation proved to work well in free-electron-like materials where the ELF  $\text{Im}[-\epsilon(0, \omega)^{-1}]$  registered for incoming photons shows a dominant peak due to well-defined volume plasmons.<sup>18,26</sup>

Similarly as above, the response of the medium to a passing electron of a given energy  $\hbar\omega$  and momentum  $\hbar\mathbf{q}$  is then described by a complex Lindhard dielectric function<sup>21</sup>  $\epsilon(\mathbf{q}, \omega)$ . In general  $\epsilon$  may be a tensor but it is assumed here that the medium is homogeneous and isotropic. In this case,  $\epsilon$  is a scalar function which depends only on the magnitude of  $\hbar\mathbf{q}$ . The probability of an energy loss  $\hbar\omega$  per unit distance traveled by a nonrelativistic electron of energy  $E$ , i.e., the differential inverse mean free path (DIMFP)  $\tau(E, \omega)$  (Refs. 21, 24, 27, and 28), then reads

$$\tau(E, \omega) = \frac{1}{\pi E a_0} \int_{q_-}^{q_+} \frac{dq}{q} \text{Im}[-\epsilon(q, \omega)^{-1}], \quad (4)$$

where  $a_0$  is the Bohr radius and

$$q_{\pm} = k[1 \pm \sqrt{1 - (\hbar\omega/E)}] \quad (5)$$

for  $k$  denoting the wave number corresponding to electron impact energy  $E$ . The expression for  $q_{\pm}$  assumes that the energy and momentum transfer for electron moving in the medium is the same as for a free particle in vacuum; i.e., there is no effective mass assumed. Integration of the DIMFP over the allowed values of  $\omega$  yields the inelastic mean free path (IMFP) through

$$\lambda_{in}^{-1}(E) = \int d\omega \tau(E, \omega). \quad (6)$$

It follows from Eq. (4) that the only quantity needed to evaluate  $\tau(E, \omega)$  and  $\lambda_{in}(E)$  is the dielectric response func-

tion  $\epsilon(q, \omega)$ . However, most existing data on dielectric response functions were obtained from photon scattering on solids, for which the momentum transfer is zero. The problem is how to predict the dielectric response function with  $q > 0$ , knowing only its optical limit ( $q = 0$ ).<sup>27,28</sup> For that purpose a phenomenological optical model approach was introduced, where  $\text{Im}[-\epsilon(q, \omega)^{-1}]$  is expressed via the convolution of  $\text{Im}[-\epsilon(q=0, \omega)^{-1}]$  with some profile function of  $q$  and  $\omega$ .

The two transparent optical models we apply hereafter were chosen to give a reasonable estimate of the ionization rate within the accuracy required for our model. In what follows we will use atomic units ( $\hbar = e = m = 1$ ) if not stated explicitly.

The optical model by Ashley<sup>27,28</sup> includes exchange between the incident electron and the electron in the medium modeled in analogy with the structure of the nonrelativistic Møller cross section:

$$\begin{aligned} \tau_A(E, \omega) = & \frac{1}{2\pi E} \int_0^\infty d\omega' \omega' \text{Im}[-\epsilon(0, \omega)^{-1}] \{ F(E, \omega', \omega) \\ & + F(E, \omega', E + \omega' - \omega) \\ & - \sqrt{F(E, \omega', \omega) F(E, \omega', E + \omega' - \omega)} \}, \end{aligned} \quad (7)$$

where

$$\begin{aligned} F(E, \omega', \omega) = & \bar{\Theta}(\omega - q_-^2/2 - \omega' > 0) \bar{\Theta} \\ & \times (\omega' + q_+^2/2 - \omega > 0) \frac{1}{\omega(\omega - \omega')}, \end{aligned} \quad (8)$$

and  $\bar{\Theta}$  is the step function. Substituting Eq. (8) into Eq. (7) one obtains<sup>27,28</sup>

$$\begin{aligned} \tau_A(E, \omega) = & \frac{1}{2\pi E} \int_0^\infty d\omega' \omega' \text{Im}[-\epsilon(0, \omega)^{-1}] \\ & \times \left( \frac{1}{\omega(\omega - \omega')} + \frac{1}{(E + \omega' - \omega)(E - \omega)} \right. \\ & \left. - \frac{1}{\sqrt{\omega(\omega - \omega')(E + \omega' - \omega)(E - \omega)}} \right) \\ & \times [\Theta_1(E, \omega', \omega) + \Theta_2(E, \omega', \omega)], \end{aligned} \quad (9)$$

where  $\Theta_1$  and  $\Theta_2$  restrict the integration region over  $\omega'$  and  $\omega$ :

$$\begin{aligned} \Theta_1(E, \omega', \omega) = & \bar{\Theta}(0 < \omega < E/2) \\ & \times \bar{\Theta}(0 < \omega' < 2E(\omega/E - 1 + \sqrt{1 - \omega/E})), \end{aligned} \quad (10)$$

$$\begin{aligned} \Theta_2(E, \omega', \omega) = & \bar{\Theta}(E/2 < \omega < 3E/4) \\ & \times \bar{\Theta}(2\omega - E < \omega' < 2E(\omega/E - 1 + \sqrt{1 - \omega/E})). \end{aligned} \quad (11)$$

The Tanuma-Powell-Penn model (TPP-2) (Ref. 18) was adopted for calculating the DIMFP and the IMFP of electrons in a solid. We have not used the TPP-2 fit for IMFP calculation but derived the DIMFP, and consequently IMFP, explicitly from the statistical approximation described in Ref. 18. The DIMFP  $\tau_T(E, \omega)$  yields

$$\begin{aligned} \tau_T(E, \omega) &= \frac{1}{2\pi E} \int_0^\infty d\omega' \omega' \text{Im}[-\epsilon(0, \omega)^{-1}] \\ &\times \frac{1}{\sqrt{c(\omega')^2 - \omega'^2 + \omega^2} [\sqrt{c(\omega')^2 - \omega'^2 + \omega^2} - c(\omega')]} \\ &\times \bar{\Theta}(q_-^2/2 < \sqrt{c(\omega')^2 - \omega'^2 + \omega^2} - c(\omega') < q_+^2/2), \end{aligned} \quad (12)$$

where  $c(\omega') = k_F(\omega')^2/3$ , and  $k_F(\omega')$  is the Fermi wave number for the free-electron gas with plasma frequency equal to  $\omega'$ :

$$k_F(\omega') = \left( \frac{3\pi}{4} \right)^{1/3} (\omega')^{2/3}. \quad (13)$$

The corresponding IMFP may be obtained after integrating Eq. (12) over  $\omega$ , according to Eq. (6), taking into account the following restrictions:

$$(q_-)^2/2 < \sqrt{c^2 - \omega'^2 + \omega^2} - c < (q_+)^2/2, \quad (14)$$

$$E - E_F < \omega, \quad (15)$$

where  $E_F$  denotes the Fermi energy (see below). In particular, restriction (14) implies  $\omega' < \omega$ . The energy loss functions for diamond and amorphous carbon used in these calculations are plotted in Figs. 2 and 3. In order to obtain the ELF for diamond, we have used optical data for diamond<sup>29,30</sup> ( $E < 35$  eV) and x-ray data for the scattering of photons on carbon<sup>31</sup> ( $E > 49.3$  eV). The ELF in the intermediate region  $35 \text{ eV} < E < 49.3$  eV was fitted in order to fulfill the oscillator-strength sum rule (3). The ELF for amorphous carbon was obtained from optical data<sup>32</sup> in the region  $E \leq 40$  eV and from x-ray data on atomic carbon<sup>31</sup> ( $E > 72.4$  eV). As previously, the ELF in the intermediate region was fitted in order to fulfill the oscillator-strength sum rule (3). Both diamond and amorphous carbon show dominant peaks in their ELF, corresponding to well-defined volume plasmons<sup>26</sup> as expected for free-electron-like materials. This means that the Lindhard dielectric function approximation describes these two solids satisfactorily.<sup>18</sup>

Figures 4 and 5 show the IMFP's of electrons in diamond and amorphous carbon, calculated from Eqs. (9) and (12). The IMFP's increase monotonically with impact energy; however, the scaling with the density of the medium is not preserved explicitly. For low energies ( $E \approx 50$  eV), the IMFP shows a characteristic rapid increase, and for the TPP-2 model it becomes undefined if approaching the Fermi energy  $E_F$  [cf. Eq. (15)].

It should be stressed that the first approximations used here give an upper limit for the total number of secondary electrons liberated by an Auger electron. We expect therefore that in reality the number of these cascade electrons will be smaller. The present model treats both allotropes of carbon (diamond, an insulator, and amorphous carbon, a conductor) as free-electron-like materials, and we model their band structure in a free-electron-gas approximation.<sup>10</sup> The Fermi energy for diamond is  $E_F = 28.7$  eV, and for amorphous carbon  $E_F = 21.1$  eV as obtained from the free-electron-gas approximation. We note that the model will give more accurate results by considering the real band structure of the solid. The Fermi level lies then in the middle of the band gap at  $T = 0$  K for semiconductors and insulators.

Based on these initial results, we have constructed a model which describes the time evolution of the secondary-electron cascade in diamond and amorphous carbon (cf. Refs. 33 and 34). The algorithm for the MC simulation is available from the authors.

The model describes the evolution of the cascade in the approximation of independent noninteracting electrons, neglecting long-range Coulomb interactions. The latter assumption holds due to the emission time scales and electron energy ranges relevant for the simulation. We assume that on average only *one* elastic or inelastic electron-atom scattering takes place in a cluster of size  $\lambda_{el(in)}$ . An electron of energy  $E$  (cf. Fig. 6) enters the solid and undergoes collisions with the atoms. Depending on the magnitude of the respective cross sections, either elastic or inelastic collisions occur as a stochastic process [probability of collision  $\approx \sigma_{el(in)}/(\sigma_{el} + \sigma_{in})$ ]. In elastic collisions, the primary electron travels through the atomic cluster of size  $\lambda_{el}(E)$  and leaves after time  $\Delta t = \lambda_{el}(E)/\sqrt{2E}$ . For an inelastic collisions the situation gets more complicated. First, as previously, the electron travels through the atomic cluster of size  $\lambda_{in}(E)$ . After time  $\Delta t = \lambda_{in}(E)/\sqrt{2E}$  it loses part of its energy  $\omega$ , and transfers it to an electron of energy  $E_0$  in the Fermi band ( $E_0 < E_F$ ). The energy  $E_0$  of the electron in the band is chosen, according to the Fermi density of levels, at  $T = 0$  K (Ref. 10) (with no thermal excitations assumed). If the total energy  $E_0 + \omega > E_F$ , the secondary electron gets excited, and it is emitted instantaneously when the primary electron leaves the cluster.

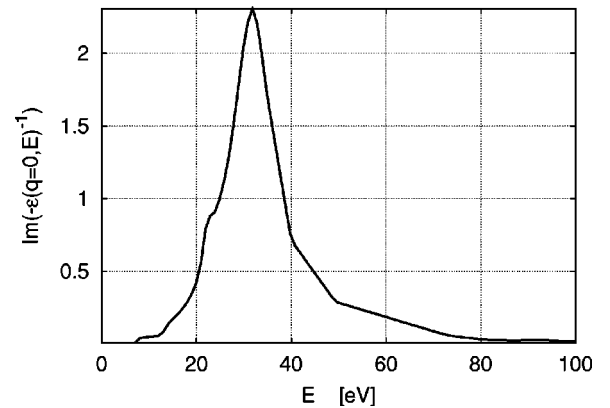


FIG. 2. Energy loss function  $\text{Im}[-\epsilon(q=0, E)^{-1}]$  for diamond plotted as a function of photon impact energy  $E$ .

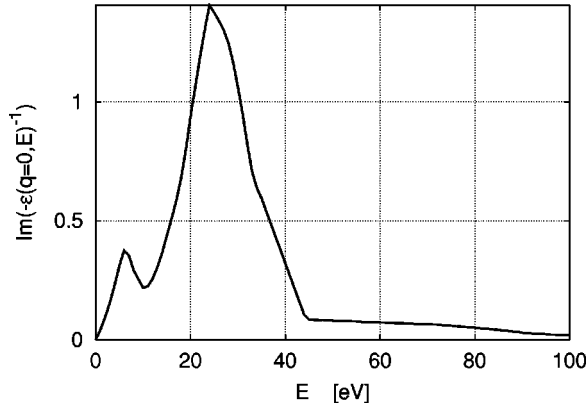


FIG. 3. Energy loss function  $\text{Im}[-\epsilon(q=0, E)^{-1}]$  for amorphous carbon plotted as a function of photon impact energy  $E$ .

Otherwise, if  $E_0 + \omega < E_F$ , the primary electron interacts inelastically with electrons in the Fermi band, losing the part of its energy  $\omega$ ; however, no secondary emission occurs in this case. The process continues until the energies of all excited electrons, including the primary one, fall below the Fermi barrier  $E_F$ .

For simplicity we have assumed here that there are no thermal excitations in the Fermi band ( $T=0$  K), and this gives an upper limit of maximal ionization. If  $T>0$ , then additional low-occupied energy levels above the Fermi energy become available, so the effective energy barrier becomes higher, and cascading will liberate fewer electrons from the Fermi band.

### III. NUMERICAL RESULTS

MC simulations showed that the number of cascade electrons converged after five iterations in both samples. A set of 500 simulations was then performed for each of the two samples in order to obtain a time-dependent estimate of the number of ionizations. In these simulations, the energy of the primary electron was fixed at  $E=E_F+250$  eV. Cascading included 1+5 interactions (the primary impact and 5 cas-

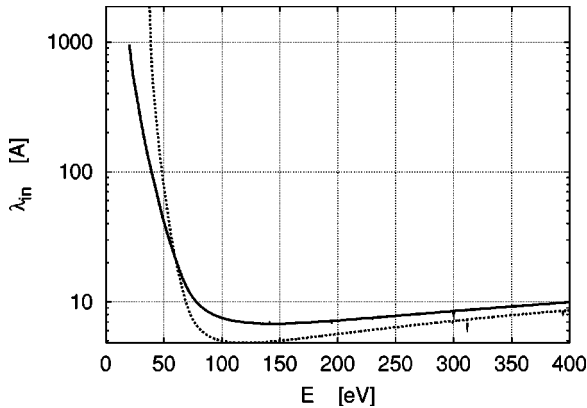


FIG. 4. Inelastic mean free path ( $\lambda_{in}$  or IMFP) of electrons in diamond plotted as a function of electron energy  $E$ . Solid line corresponds to the IMFP calculated from Ashley's model (9); dotted line shows the IMFP calculated from the TPP-2 model (12).

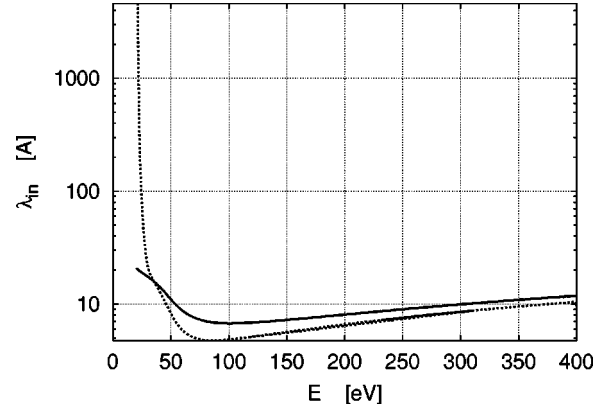


FIG. 5. Inelastic mean free path ( $\lambda_{in}$  or IMFP) of electrons in amorphous carbon plotted as a function of electron energy  $E$ . Solid line corresponds to the IMFP calculated from Ashley's model (9); dotted line shows the IMFP calculated from the TPP-2 model (12).

cade steps). Figure 7 shows the results.

For diamond the average number of ionization events after the first femtosecond was estimated to be  $\approx 6$  based on Ashley's model (9) and  $\approx 7$  based on the TPP-2 model (12). The number of secondary ionizations increased with time, and it saturated within about 40 fs with a total of 37 electrons released at the maximal ionization of  $\approx 37$  events (Ashley). Saturation was slower with the TPP-2 model (100 fs), and the total number of cascade electrons (about 18) was about the half of those ejected in Ashley's model. It should be stressed that in the latter case (TPP-2) the average number of ionizations grew slowly with time. The same scenario held also for the cascades in amorphous carbon. Both Ashley's and the TPP-2 models predicted 6–8 ionizations after the first femtosecond. Calculations based on Ashley's model give a total number of around 40 cascade electrons. These electrons were released within the first 10 fs, after which no more ionizations occurred. Calculations based on the TPP-2 model level out at 100 fs, and the total number of electrons released in the cascade is only about 23.

The IMFP at  $E=250+E_F$  eV calculated from Eq. (9) (Ashley) was larger than the corresponding IMFP from the TPP-2 model (12) for both diamond and amorphous carbon. However, the most probable energy loss at this energy is less than 60 eV in 80% of the cases as estimated from the integrated energy loss probability density. This implies that the subsequent cascade is dominated by secondary electrons of

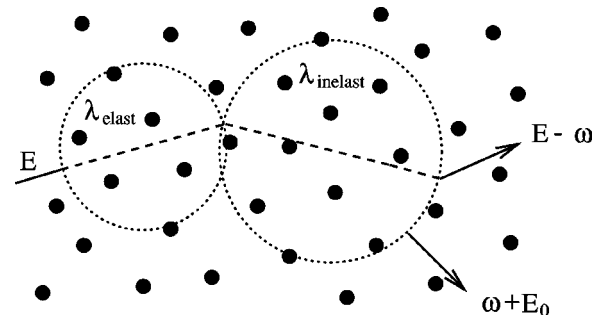


FIG. 6. Example of an electron path in a solid.

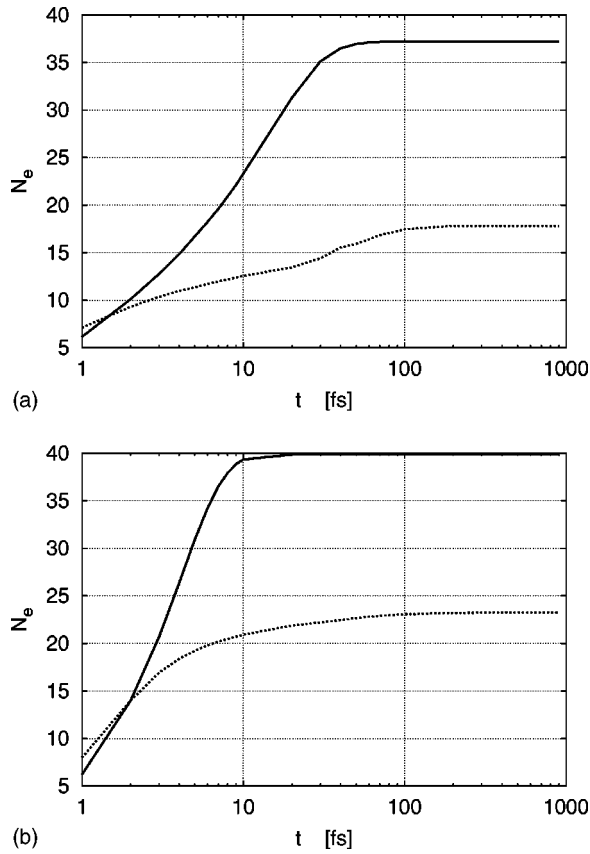


FIG. 7. The average ionization rate  $N_e$  plotted as a function of time  $t$  for diamond (upper plot) and for amorphous carbon (lower plot). The energy of the primary Auger electron was  $E = 250 + E_F$  eV, where  $E_F$  is the Fermi energy:  $E_F \approx 29$  eV for diamond and  $E_F \approx 21$  eV for amorphous carbon. Solid lines correspond to the average ionization estimated from Ashley's model; dotted lines show the average ionization calculated from the TPP-2 model.

energy 60 eV and less, and at this energy, the IMFP calculated in the TPP-2 model is larger than the IMFP in Ashley's model. Therefore, the number of ionizations estimated in Ashley's model is larger for both diamond and amorphous carbon.

We have also plotted the maximal average ionization as the function of the electron impact energy (cf. Fig. 8). The total number of ionizations increases linearly with impact energy in the energy range between  $100 + E_F$  eV and  $300 + E_F$  eV, as expected.

In constructing the model, we laid emphasis on formulating a reliable description of the Auger electron passage through a solid. Therefore we restricted ourselves to an estimation of the upper limit of ionizations caused by a single Auger electron. This approach allowed us to use first-order approximations to model electron-solid interactions. We performed our calculations in the approximation of noninteracting electrons in the cascade, neglecting long-range Coulomb interactions. Since the maximal number of ions in the carbonic medium caused by a single primary Auger electron is small ( $\approx 20$ – $40$ ) in comparison with the total number of atoms in the sample [ $\approx 10^9$  atoms for  $(100 \times 100 \times 100)$  nm<sup>3</sup> cube], the approximation of neutral atoms for

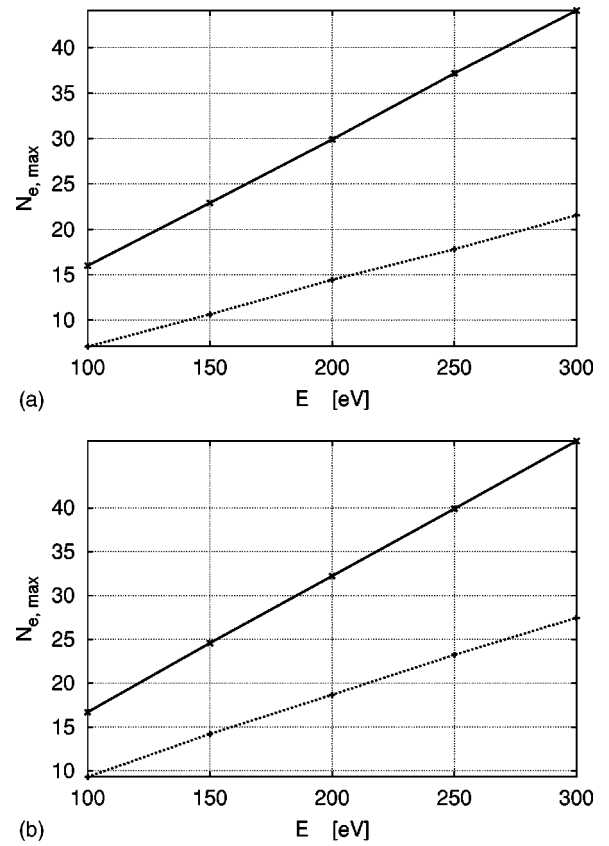


FIG. 8. Maximal ionization rate  $N_{e,max}$  plotted as a function of the energy of the primary Auger electron,  $E = E' + E_F$  ( $E' = 100, 150, 200, 250, 300$  eV), for diamond (upper plot) and for amorphous carbon (lower plot). The corresponding Fermi energies are  $E_F \approx 29$  eV for diamond and  $E_F \approx 21$  eV for amorphous carbon. Solid lines show the maximal ionization estimated from Ashley's model; dotted lines show maximal ionization calculated from the TPP-2 model.

which the values for the IMFP, EMFP, and DIMFP were derived is supposed to work well. This approach is expected to be useful for any secondary-electron cascade generated by Auger electrons released in photoelectric events.

Moreover, for microscopic samples one may neglect the ionization rate caused by a photoelectron and then approximate the total ionization rate caused by a single photoelectric event by the Auger-electron ionization rate. This translates into an ionization rate of  $\approx 20$ – $40$  secondary electrons emitted within the first 100 femtoseconds after the primary electron emission in diamond and amorphous carbon.

Finally, it should be stressed that we modeled the band structure of diamond and amorphous carbon using a free-electron-gas approximation. This assumption gives an upper estimation of the ionization rate caused by a single Auger electron. Moreover, secondary-electron emission was considered in the case of  $T = 0$  K (with no thermal excitations in the Fermi band), and this, again, overestimates the maximal number of ionizations. At  $T > 0$  K, the effective energy barrier becomes higher, and cascading will excite fewer electrons from the Fermi band than in the case of  $T = 0$  K.

If one considers the real band structure of the solid, then

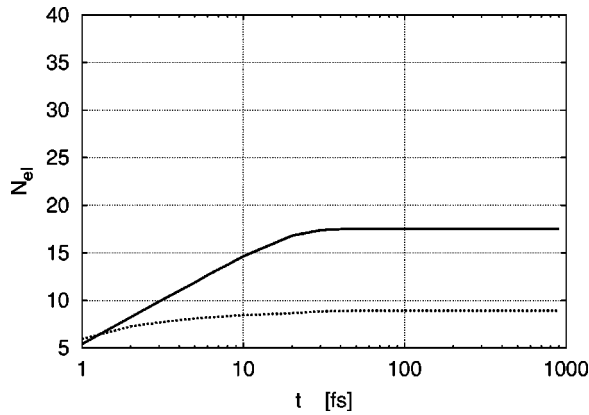


FIG. 9. The average ionization rate  $N_e$  plotted as a function of time  $t$  for diamond after the real band structure of diamond at  $T = 300$  K was included in the model. The energy of the primary Auger electron was  $E = 250 + E_F$  eV, where  $E_F$  is the Fermi energy:  $E_F \approx 29$  eV for diamond. The energy gap at  $T = 300$  K equals  $E_{gap} = 5.46$  eV. Solid lines correspond to the average ionization estimated from Ashley's model; dotted lines show the average ionization calculated from the TPP-2 model.

the expected total number of electrons ejected in the cascade decreases further as the Fermi level lies in the middle of the band gap at  $T = 0$  K (semiconductors and insulators). The effect of including the real band structure on the ionization dynamics is shown in Fig. 9 for diamond, for which the band structure is well established.<sup>35–37</sup>

#### IV. CONCLUSIONS

The primary photoelectrons and the Auger electrons may escape from very small samples; however, in larger samples, these electrons may become trapped and thermalized. This process leads to additional ionization and to the deposition of further energy into the sample. Thermalization involves inelastic electron-atom interactions and produces secondary cascade electrons on a longer time scale. In this paper, we analyzed the specific contribution of Auger electrons to the overall ionization of a macroscopic sample. The results describe the evolution of Auger-electron cascades in two model compounds, diamond and amorphous carbon, and show that a maximum of 20–40 secondary cascade electrons may be released by a single Auger electron within the first 100 fs following the emission of the Auger electron. A quantitative description of the ionization dynamics of target samples is of crucial importance to practically all planned experiments at x-ray free-electron lasers, ranging from imaging to the creation of warm dense matter.

#### ACKNOWLEDGMENTS

We are grateful to Gyula Faigel, Zoltan Jurek, Michel A. van Hove, Leszek Motyka, Richard Neutze, and Remco Wouts for discussions. This research has been supported in part by the Polish Committee for Scientific Research with Grant Nos. 2 P03B 04718 and 2 P03B 05119, the EU-BIOTECH Programme, and the Swedish Research Councils. A.S. was supported by STINT. B.Z. was supported by the Wenner-Gren Foundations.

\*Electronic address: ziaja@tsl.uu.se

†Electronic address: spoel@xray.bmc.uu.se

‡Electronic address: szoke1@lml.gov

§Corresponding author. FAX: +4618 511755. Electronic address: hajdu@xray.bmc.uu.se

<sup>1</sup>R. Henderson, Q. Rev. Biophys. **28**, 171 (1995).

<sup>2</sup>R. Henderson, Proc. R. Soc. London Biol. Sci. **241**, 6 (1990).

<sup>3</sup>C. Nave, Radiat. Phys. Chem. **45**, 483 (1995).

<sup>4</sup>J. Hajdu, K. Hodgson, J. Miao, D. van der Spoel, R. Neutze, C. V. Robinson, G. Faigel, C. Jacobsen, J. Kirz, D. Sayre, E. Weckert, G. Materlik, and A. Szoke (unpublished).

<sup>5</sup>J. Hajdu and E. Weckert (unpublished).

<sup>6</sup>R. Neutze, R. Wouts, E. van der Spoel, E. Weckert, and J. Hajdu, Nature (London) **406**, 752 (2000).

<sup>7</sup>J. Hajdu, Curr. Opin. Struct. Biol. **10**, 569 (2000).

<sup>8</sup>N. A. Dyson, *X-rays in Atomic and Nuclear Physics* (Longman, London, 1973).

<sup>9</sup>M. O. Krause and J. H. Oliver, J. Phys. Chem. Ref. Data **8**, 329 (1979).

<sup>10</sup>N. W. Ashcroft and N. D. Mermin, *Solid State Physics* (Harcourt, New York, 1976).

<sup>11</sup>B. H. Bransden and C. J. Joachain, *Physics of Atoms and Molecules* (Longman, Essex, 1998), pp. 505–513.

<sup>12</sup>P. G. Burke, *Atomic, Molecular, and Optical Physics Handbook*, edited by G. W. F. Drake (AIP, Woodbury, NY, 1996), p. 536.

<sup>13</sup>C. J. Powell, J. Electron Spectrosc. Relat. Phenom. **47**, 197 (1988).

<sup>14</sup>S. Tanuma, C. J. Powell, and D. R. Penn, Surf. Interface Anal. **17**, 911 (1991).

<sup>15</sup>J. J. Rehr and R. C. Albers, Phys. Rev. B **41**, 8139 (1990).

<sup>16</sup>J. C. Ashley, J. Electron Spectrosc. Relat. Phenom. **46**, 199 (1988).

<sup>17</sup>A. Barbieri and M. A. Van Hove (private communication); Phase Shift Package, <http://electron.lbl.gov/leedpack/>

<sup>18</sup>S. Tanuma, C. J. Powell, and D. R. Penn, Surf. Interface Anal. **11**, 577 (1988).

<sup>19</sup>E. Fermi, Z. Phys. **29**, 315 (1924).

<sup>20</sup>D. Pines and D. Bohm, Phys. Rev. **85**, 338 (1952).

<sup>21</sup>J. Lindhard, K. Dan. Vidensk. Selsk. Mat. Fys. Medd. **28**, 1 (1954).

<sup>22</sup>J. Hubbard, Proc. R. Soc. London, Ser. A **68**, 976 (1955).

<sup>23</sup>P. Nozières and D. Pines, Nuovo Cimento **9**, 470 (1958).

<sup>24</sup>R. H. Ritchie, Phys. Rev. **114**, 644 (1959).

<sup>25</sup>I. Abril, R. Garcia-Molina, C. D. Denton, F. Pérez-Pérez Javier, and N. R. Arista, Phys. Rev. A **58**, 357 (1998).

<sup>26</sup>D. R. Penn, Phys. Rev. B **13**, 5248 (1976).

<sup>27</sup>J. C. Ashley, J. Electron Spectrosc. Relat. Phenom. **50**, 323 (1990).

<sup>28</sup>J. C. Ashley, J. Appl. Phys. **69**, 674 (1991).

<sup>29</sup>D. F. Edwards and H. R. Philipp, in *Handbook of Optical Constants of Solids*, edited by E. D. Palik (Academic, New York, 1985), p. 666.

<sup>30</sup>H. R. Philipp and E. A. Taft, Phys. Rev. **136**, 1445 (1964).

<sup>31</sup>B. L. Henke, E. M. Gullikson, and J. C. Davis, At. Data Nucl. Data Tables **54**, 211 (1993).

<sup>32</sup>J. Cazaux and D. Gramari, J. Phys. (Paris) **38**, L133 (1977).

<sup>33</sup>K. Nishimura, J. Kawata, and K. Ohya, Nucl. Instrum. Methods

- Phys. Res. B **164–165**, 903 (2000).
- <sup>34</sup>S. Tanuma, S. Ichimura, and K. Yoshihara, Appl. Surf. Sci. **100/101**, 47 (1996).
- <sup>35</sup>M. Rohlfing, P. Krüger, and J. Pollmann, Phys. Rev. B **48**, 17 791 (1993).
- <sup>36</sup>I. Jiménez, L. J. Terminello, D. G. J. Sutherland, and J. A. Carlisle, Phys. Rev. B **56**, 7215 (1997).
- <sup>37</sup>Database on Semiconductors, <http://www.ioffe.rssi.ru/SVA/NSM/Semicond/>